

Journal of Mechanics of Materials and Structures

**ON THE MODELING OF DISSIPATIVE MECHANISMS IN A
DUCTILE SOFTENING BAR**

Jacinto Ulloa, Patricio Rodríguez and Esteban Samaniego

Volume 11, No. 4

July 2016



ON THE MODELING OF DISSIPATIVE MECHANISMS IN A DUCTILE SOFTENING BAR

JACINTO ULLOA, PATRICIO RODRÍGUEZ AND ESTEBAN SAMANIEGO

The computational modeling of softening materials is still a challenging subject. An interesting way to deal with this problem is to adopt a variational framework. However, there are appealing features in using a classical approach. We explore the possibilities of both frameworks to include dissipative mechanisms. We start with a one-dimensional variational plastic-damage model rewritten in a classical framework, where regularization through viscoplasticity is applied. We highlight the appearance of an implicit internal length in the plastic strain field during the damage phase, allowing plasticity to evolve over a region before concentrating. Then, a consistent variational approach is adopted. A plastic strain gradient term is added to the global energy functional, with variable internal length coupled to the damage level. This model is further enriched by the addition of a hardening variable to the plastic evolution. A comparative analysis of the computational implementation of the different alternatives is performed.

1. Introduction

Classical fracture mechanics models are noteworthy for the description of existing cracks; however, the precursory state of the material is not provided by these theories [Lemaitre and Lippmann 1996]. Hence, the introduction of damage mechanics plays a major role in the representation of the evolution previous to the eventual macroscopic crack. According to Krajcinovic [1989], the deterioration of a material can be described in at least three levels of scale. The treatment of the first, corresponding to the atomic level, requires noncontinuum mechanics. The second level is related to the formation of microcracks and microvoids and is treated via continuum damage mechanics. On the other hand, the third scale corresponds to the macroscopic level and is treated by classical fracture models. In this work, the second level of scale is considered, and the softening mechanism of damage is coupled to plasticity to capture ductile failure. Furthermore, the thermodynamics of internal variables is applied to build the model in a physically consistent manner, which stems out from [Maugin 1992; Maugin and Muschik 1994]. Representing ductile behavior in a softening regime is a challenging task that has not been widely explored in past efforts in a variational setting [Ambati et al. 2015]. For a comprehensive account of material failure, the reader is referred to [Bigoni 2012].

The capacity to simulate the strain localization phenomenon and hence, the appearance of discontinuities in the displacement field that characterizes fracture, is an attractive feature of local softening models [Oliver et al. 2002]. However, its use has been known to result in ill-posed problems, returning mesh-dependent solutions and spurious localization, which are meaningless material responses [De Borst and Mühlhaus 1992]. This problem has been widely treated and several methods have been employed.

Keywords: material modeling, dissipative materials, plasticity, damage, classical approach, variational formulation.

Relying on the introduction of discontinuous functions in the description of the displacement field, several techniques have shown fruitful results. The strong discontinuity approach and the extended finite element method discussed in [Oliver et al. 2002; 2003; Moës et al. 1999] have been applied to the modeling of fracture and strain concentration in [Oliver et al. 2004; Chen et al. 2011; Samaniego and Belytschko 2005]. Another interesting treatment can be seen in the multiple scale analytical approach found in [Garikipati and Hughes 1998]. The concept is applied in an adaptive-mesh strategy for a local plastic-damage model in [Venini and Morana 2001].

In other approaches, modifications to the constitutive equations are made to include nonlocal effects, ranging from rate-dependent viscoplastic regularization (see [Needleman 1988]) to gradient-enhanced models, where nonlocal treatments furnish fruitful results (see [Bažant and Jirásek 2002] for nonlocal formulations). All of these are, to some degree, based on the introduction of an internal length scale as a material's characteristic property [Borst et al. 1993].

The application of regularization to simulate fracture is of great interest and has been treated in several works. The introduction of a gradient term was first proposed in [Triantafyllidis and Aifantis 1986], and has been widely applied to nonlocal energy functionals. The derivation of a gradient regularization for a phase-field fracture model can be seen in [Miehe et al. 2010]. A phase-field model for ductile fracture is proposed in [Ambati et al. 2015]. Softening gradient-dependent plasticity models are analyzed in [Jirásek and Rolshoven 2009a; 2009b], and with verification of experimental results in [Lancioni 2015]. Both gradient-dependent plasticity and gradient-dependent damage models are analyzed in [de Borst et al. 1999]. Furthermore, gradient-dependent variational models are proven to converge to the Griffith fracture model in [Bourdin et al. 2008] through Γ convergence. Thus, regularization via the internal length represents the transition between discontinuous fracture models and regularized models [Ambati et al. 2015]. On the other hand, a viscoplastic regularization of local damage can be seen in [Niazi et al. 2013] and a study of a model that includes rate-dependent perturbations and gradient terms is carried out in [Dal Corso and Willis 2011].

This work picks up from the variational gradient damage model coupled to perfect plasticity proposed by Alessi [2013; 2014], which was initially developed in [Pham and Marigo 2010a; 2010b] for brittle fracture. The variational approach follows the regularization of [Bourdin et al. 2008] for the energy minimization approach of the Griffith model that was proposed in [Francfort and Marigo 1998]. The energetic formulation that is applied comes from [Mainik and Mielke 2005; Mielke 2006] for rate-independent systems. As pointed out in [de Borst et al. 1999], the coupling of plasticity to damage is physically appealing due to the capability of representing a wide range of materials that deteriorate with a combination of void nucleation and plastic strains. The model in [Alessi 2013; Alessi et al. 2014] is capable of capturing different behaviors, from where we highlight the following evolution:

- (1) An initial elastic phase.
- (2) A homogeneous perfect plasticity phase.
- (3) A plasticity and damage coupled phase with a strain localization region, where a jump in the displacement field appears with nonvanishing stress. Then, a cohesive crack forms at the center of the localization zone.

The variational formulation furnishes a natural numerical implementation that results in an *alternate minimization algorithm*, which is applied to minimize a global energy functional [Mumford and Shah

1989]. However, the use of global energy functionals could lead to nonphysical results [Bourdin et al. 2008]. For instance, a homogeneous damage evolution, which is possible in this context, would be a clearly nonphysical response for a deteriorating material. Despite this, several advantages of this treatment are observed in this work. For example, plasticity is able to evolve uniformly during the perfect plasticity phase, without a regularization method [Alessi 2013]. Contrary to the classical approach, the variational model conserves the local constitutive equations without the necessity of introducing nonlocal effects in this stage.

In this work, this model is rewritten in a classical framework, where the evolution of the system is defined using the algorithm discussed in [Simo and Hughes 1998]. Here, the balance of the linear momentum equation is solved to determine the displacement field over the body. In this approach, it becomes evident that the perfect plasticity model lacks uniqueness and requires local regularization. In order to conserve the structure of the algorithm in [Simo and Hughes 1998] and to maintain a local definition of the plastic variables (see [Borja 2013] and [Runesson 2006] for local plasticity and damage formulations), the viscoplasticity model, also discussed in [Simo and Hughes 1998], is adopted instead of the perfect plasticity model. Although rate-dependence is introduced in the evolution of the system with this regularization, it is shown numerically that as the loading rate tends to zero, the response converges to the variational model in [Alessi 2013]. One feature observed in the simulations of the viscoplastic regularized evolution is worth highlighting: the appearance of an implicit internal length scale in the plastic strain field that varies with the loading rate. As we will see in Section 4, this allows plasticity to evolve over a determined region during the plasticity-damage phase.

To develop this feature in a more consistent manner, and taking advantage of the capacity of the variational approach to incorporate new characteristics in the model by (eventually) adding new terms to the global energy functional, the following original contributions are incorporated in this work:

- (1) The addition of a hardening variable coupled to damage to capture additional material responses and the analysis of the resulting local evolution.
- (2) The addition of a plastic strain gradient term to the global model.
- (3) The application of a variable plastic strain internal length depending on the damage variable. A threshold damage level is introduced to control when the plastic internal length drops to zero.
- (4) The numeric solution of the complete gradient-dependent damage and gradient-dependent hardening plasticity model.

The first new feature enables the model to capture material behaviors with a hardening plastic phase, which is common in metals. Then, the incorporation of the plastic strain gradient term allows plasticity to evolve in a controlled region via the internal length. If Neumann boundary conditions are imposed on the plastic strain field, plasticity will first evolve homogeneously, and Dirichlet boundary conditions are necessary on the damage field to trigger a nonhomogeneous evolution. As pointed out in [Bigoni 2012], several material evolutions initially present a homogeneous deformation, until bifurcation and instabilities appear. Then, only after extreme loading, strain localizations take place. In this case, these are due to plasticity and damage and a localized response is not induced until softening occurs in the damage phase. In the case of Neumann bounded plasticity, the distribution of plastic strains remains homogeneous until softening. Similar results have been obtained in [Dal Corso and Willis 2011] for

an approach involving perturbations, where plastic strains begin to localize in the defects during the softening regime. Then, the plastic strain internal length is allowed to vary as a decreasing function of the damage level, simulating the necking phenomenon of a deteriorating material with strain localization. Moreover, the damage threshold value deactivates the effect of the plastic internal length when desired, changing the jump in the displacement field from a relatively smooth behavior to an abrupt evolution and localizing the plastic strains at the center of the bar. It is worth mentioning that the plastic strain gradient does not replace the damage gradient and both terms are used. This is because a local damage evolution will cause an abrupt localization of damage and an instantaneous rupture as soon as the damage phase begins.

The main novelty of this work lies in the fact that the mechanisms described above have been carefully added within a thermodynamically consistent variational framework, enriching the model presented in [Alessi 2013], which only considers local perfect plasticity and gradient damage. A similar effort can be found in [Ambati et al. 2015], which builds over [Duda et al. 2015]. There, gradient damage is coupled to hardening plasticity by heuristically modifying the original energy functional. By contrast, in our contribution, new coupling terms and a new gradient term (gradient plasticity with a variable internal length) are consistently added within the same rigorous framework used to build the model in [Alessi 2013]. Additionally, the problem has been treated in a classical setting with viscoplasticity, and the numerical solution for both frameworks is presented. The results of the time-dependent model are qualitatively compared to the variational model with gradient-enhanced plasticity.

The first section of this work consists of the classical formulation of the elastic-plastic-damage problem. The standard local models for perfect plasticity and viscoplasticity, as well as the numeric implementation of the global response are briefly explored. Then, the gradient-dependent damage model is coupled to the elastic-plastic evolution, and the computational implementation is presented, where the finite element method is used with linear approximations on the displacement and damage fields. The next section is devoted to the explicit enrichment of the variational model. First, the hardening variable is added to the local evolution and the resulting response is analyzed. Then, the plastic strain gradient term is added to the nonlocal functional. The resulting formulation is solved through the finite element method with quadratic approximations on the displacement field, and the computational implementation is presented. For both approaches, the model is implemented in a one-dimensional fashion for a bar with Dirichlet boundary conditions: one end is constrained and displacements are imposed on the other. For simplicity and without losing generality, an initially virgin material is considered and only monotonic loading is applied. The small strain theory is applied, and the decomposition of the total strain,

$$\epsilon = \epsilon_e + \epsilon_p,$$

is considered, where ϵ_e and ϵ_p are the elastic and plastic strains, respectively.

2. Classical approach

This section is devoted to the classical formulation of the plastic-damage model in [Alessi 2013]. Although mathematically equivalent to the energetic formulation for the plastic-damage response, the classical approach leads to a different numerical model. While the damage field is still given by the nonlocal

gradient criterion, both the displacement field and the plastic strain field are found simultaneously by the standard Newton–Raphson method, which can be found in [Simo and Hughes 1998; Borja 2013].

As mentioned, the problem of perfect plasticity in a classical approach requires regularization. The Newton–Raphson method distributes the displacements along the bar by obtaining the plastic strain field locally via a standard *return mapping algorithm* and verifying equilibrium. Thus, once the yield stress is reached, there is an infinite number of admissible solutions. Specifically, strains localize in the element where the displacement is imposed. Because of this, a viscoplastic model is used as a regularization to approximate the perfect plasticity phase.

2.1. Perfect plasticity model and viscoplastic regularization.

2.1.1. Governing equations. The perfect plasticity and viscoplastic models that are briefly explored can be seen in [Simo and Hughes 1998; Runesson 2006], and the numeric implementation is developed in [Simo and Hughes 1998]. The free energy is defined locally as

$$\Psi(\epsilon, \epsilon_p) = \frac{1}{2} E (\epsilon - \epsilon_p)^2, \quad (2-1)$$

with E as the elastic modulus, from where the constitutive equations

$$\sigma = \frac{\partial \Psi}{\partial \epsilon} = E(\epsilon - \epsilon_p), \quad \sigma_p = -\frac{\partial \Psi}{\partial \epsilon_p} = E(\epsilon - \epsilon_p) \equiv \sigma,$$

are obtained. The quasistatic yield criterion is defined as

$$f(\epsilon, \epsilon_p) = f(\sigma) = |\sigma| - \sigma_p, \quad (2-2)$$

where σ_p is the initial yield stress. In the case of rate-independent plasticity, one has $f(\epsilon, \epsilon_p) \leq 0$. Hence, after defining the plastic multiplier $\lambda = |\dot{\epsilon}_p|$, the Kuhn–Tucker conditions

$$\lambda \geq 0, \quad f(\sigma) \leq 0, \quad \lambda f(\sigma) = 0, \quad (2-3)$$

follow. The actual value of the plastic multiplier λ is found via the consistency conditions and the plastic flow rule, which reads as

$$\dot{\epsilon}_p = \lambda \frac{\partial}{\partial \sigma} f(\sigma) = \lambda \text{sign } \sigma. \quad (2-4)$$

The consistency conditions are a function of $\dot{f}(\sigma)$, where one has

$$\dot{f}(\sigma) \leq 0, \quad \lambda \geq 0, \quad \dot{f}(\sigma) \lambda = 0. \quad (2-5)$$

The plastic response is then given by equations (2-3), (2-4) and (2-5).

On the other hand, the yield criterion defined in (2-2) is allowed to exceed the yield surface for the viscoplastic model, where $|\sigma| > \sigma_p$. The additional stress is accounted for by the *overstress*, defined as

$$\sigma_{\text{ex}} = (|\sigma| - \sigma_p) \text{sign}(\sigma) = f(\sigma) \text{sign}(\sigma).$$

Defining the viscous relationship $\sigma_{\text{ex}} = \nu \dot{\epsilon}_p$, where ν is the viscosity constant, the evolution of the plastic strain is given by

$$\dot{\epsilon}_p = (\sigma - \sigma_p) / (E \tau),$$

where $\tau = \nu/E$ is the relaxation time, which can be interpreted as a factor that determines the rate at which the overstress tends to zero and the stress tends to the yield stress, recovering the plastic rate-independent response.

These models are solved computationally in a discrete fashion, where the state of the system is given at time n by the set of variables $(\sigma_n, \epsilon_{p_n})$, and the goal is to determine the updated variables $(\sigma_{n+1}, \epsilon_{p_{n+1}})$ at time $n + 1$ via standard *return mapping algorithms*. The steps are summarized in the local algorithms found in [Simo and Hughes 1998].

2.1.2. Energy dissipation. From the Clausius–Duhem inequality, one has

$$\sigma \dot{\epsilon} - \dot{\Psi} \geq 0$$

which, for the viscoplastic model, leads to

$$\Phi = |\dot{\epsilon}_p|(\sigma_p + \sigma_{ex}) = |\dot{\epsilon}_p|\sigma_p(1 + \nu|\dot{\epsilon}_p|/\sigma_p) \geq 0.$$

Again, note that as ν tends to zero, the dissipation potential tends to the rate-independent plastic potential, which reads as

$$\Phi = |\dot{\epsilon}_p|\sigma_p.$$

2.1.3. Global iterative solution. Once the local evolution is defined, the global response is obtained through the finite element method in a Newton–Raphson iterative procedure.

Consider a one-dimensional body occupying a space $\Omega = [0, L]$. The initial boundary-value problem is defined by the boundary conditions, which are only imposed in the displacement field:

$$u(0, t) = 0, \quad u(L, t) = \bar{u}(t) \quad \forall t \in [0, T],$$

where $\bar{u}(t)$ is the imposed displacement and $t \in [0, T]$ is an arbitrary time in the interval where displacements are imposed.

The initial boundary-value problem stems out from the balance of linear momentum, and reads as

$$\rho \frac{\partial v}{\partial t} - b_f - \frac{\partial \sigma}{\partial x} = 0.$$

The first term is eliminated once the dynamic effects have been neglected and the second term equals zero once the absence of external loads has been considered. Then, after introducing the test function w , with $w|_0^L = 0$, the weak form is

$$\int_0^L \sigma \frac{\partial w}{\partial x} dx = 0. \tag{2-6}$$

The approximation functions $w^h(x) = \sum_{i=1}^n w_i N_i(x)$ and $\sigma^h(x, t)$ are considered, with shape functions contained in vectors N and $B = dN/dx$. Then, from (2-6), the matrix form of the problem is

$$\int_0^L w^T \sigma^h B^T dx = w^T \int_0^L \sigma^h B^T dx = w^T [F^{int}] = 0$$

which, because of the boundary conditions in w , results in

$$\mathbf{R} = \begin{bmatrix} F_2^{\text{int}} \\ \vdots \\ F_{n-1}^{\text{int}} \end{bmatrix} = 0. \quad (2-7)$$

In the case of a linear elastic response, the stress field is simply given by $\sigma = E\epsilon$. On the other hand, a nonlinear behavior is given by nonlinear local models, such as the constitutive models explored in the previous section. The global response is then obtained through the iterative Newton–Raphson procedure, which can be found in [Simo and Hughes 1998; Borja 2013]. Essentially, a displacement vector is found that results in a convergence vector given by (2-7) and meets a certain tolerance.

2.2. Damage coupling. In this section, the damage criterion is presented in a classical framework, where the evolution of the damage variable $\alpha \in [0, 1)$ is coupled to the plastic evolution. The damage criterion can be expressed as

$$f_d = a(\hat{\sigma}) - g(\alpha, p, \alpha'') \leq 0,$$

where a is the dissipative force of the damage variable, $\hat{\sigma}$ is the effective stress, which stems out from the equivalent strain principle, and $p = \int_0^t |\dot{\epsilon}_p(x, \tau)| d\tau$ is the accumulated plastic strain. The criterion is expressed as

$$f_d = a(\hat{\sigma}) - w'(\alpha) + pm(\alpha) + \eta_d^2 \alpha'' \leq 0, \quad (2-8)$$

where $w(\alpha)$ is related to the damage dissipation and η_d corresponds to the internal length. The term $m(\alpha)$ allows the coupling between damage and plasticity, where $m(\alpha) > 0 \forall \alpha \in [0, 1)$ is defined. Equation (2-8) has been adopted from [Alessi 2013] and represents the nonlocal damage criterion that is solved through the finite element method. As in [Alessi 2013], the constitutive functions

$$E(\alpha) = E_0(1 - \alpha)^2, \quad w(\alpha) = w_o\alpha, \quad m(\alpha) = -\sigma'_{p_0}(\alpha), \quad \sigma_p(\alpha) = \sigma_{p_0}(1 - \alpha)^2, \quad (2-9)$$

are applied, where E_0 is the initial elastic modulus and σ_{p_0} is the initial plastic yield stress. Replacing in (2-8),

$$f_d = E_o(\epsilon - \epsilon_p)^2(1 - \alpha) - w_o + 2\sigma_{y_o}(1 - \alpha)p + \eta_d^2 \alpha'' \leq 0.$$

The first term in the previous expression corresponds to the dissipative force $a(\hat{\sigma})$. It is the result of taking the derivative of the free energy with respect to the damage variable once the damage effect $(1 - \alpha)^2$ has been multiplied by the elastic modulus in (2-1). The effective stress takes the form $\hat{\sigma} = \sigma/(1 - \alpha)^2$. In order to break the homogeneity of the bar, the Dirichlet boundary conditions

$$\alpha(0, t) = \alpha(L, t) = 0$$

are applied. Additionally, a response capable of recovering stiffness is not considered; hence, the irreversibility condition

$$\alpha(t_i) \leq \alpha(t_j) \forall i \leq j \quad (2-10)$$

is applied. The weak form of the damage criterion reads as

$$\int_0^L E_o(1 - \alpha)(\epsilon - \epsilon_p)^2 w \, dx - \int_0^L w_o w \, dx + \int_0^L 2\sigma_{y_o}(1 - \alpha) p w \, dx + \int_0^L \eta_d^2 \frac{\partial^2 \alpha}{\partial x^2} w \, dx = 0,$$

which leads to the following matrix form:

$$\begin{aligned} \mathbf{w}^T \int_0^L \mathbf{N}^T E_o (\epsilon - \epsilon_p)^2 dx - \mathbf{w}^T \int_0^L \mathbf{N}^T E_o (\epsilon - \epsilon_p)^2 N dx \boldsymbol{\alpha} - \mathbf{w}^T \int_0^L \mathbf{N}^T w_o dx \\ + \mathbf{w}^T \int_0^L 2\sigma_{y_o} p N^T dx - \mathbf{w}^T \int_0^L 2\sigma_{y_o} p N^T N dx \boldsymbol{\alpha} - \mathbf{w}^T \int_0^L \mathbf{B}^T \eta_d^2 \mathbf{B} \boldsymbol{\alpha} dx = 0. \end{aligned}$$

The following vectors and matrices are obtained:

$$\begin{aligned} \mathbf{E}_d &= \int_0^L \mathbf{N}^T E_o (\epsilon - \epsilon_p)^2 dx, & \mathbf{L}_d &= \int_0^L \mathbf{N}^T E_o (\epsilon - \epsilon_p)^2 N dx, \\ \mathbf{W}_d &= \int_0^L \mathbf{N}^T w_o dx, & \mathbf{S}_d &= \int_0^L 2\sigma_{y_o} p N^T dx, \\ \mathbf{M}_d &= \int_0^L 2\sigma_{y_o} p N^T N dx, & \mathbf{J}_d &= \int_0^L \mathbf{B}^T \eta_d^2 \mathbf{B} \boldsymbol{\alpha} dx, \end{aligned}$$

from where the nodal values of $\boldsymbol{\alpha}$ are obtained as

$$\boldsymbol{\alpha} = [-\mathbf{J}_d - \mathbf{L}_d - \mathbf{M}_d]^{-1} [\mathbf{W}_d - \mathbf{S}_d - \mathbf{E}_d]. \quad (2-11)$$

2.3. Computational implementation. The elastic-plastic response in [Section 2.1.3](#). is coupled to the damage evolution, where the plastic yield surface is now

$$f_p = |\sigma| - \sigma_p(\boldsymbol{\alpha}) \leq 0,$$

and the stress is $\sigma = E(\boldsymbol{\alpha})(\epsilon - \epsilon_p)$. The global elastic-plastic-damage response is obtained with the following considerations:

- The displacements are imposed gradually, where n_{desp} is the number of imposed displacements.
- Two convergence criteria are applied: the sum of the internal forces with tolerance tol_p for the elastic-plastic problem and L_∞ norm with tolerance tol_d for the damage problem.

The procedure is presented in [Algorithm 1](#), which resembles the procedure used in [\[Almansba et al. 2010\]](#).

3. Variational approach

This section is devoted to the enrichment of the variational plastic-damage model in [\[Alessi 2013\]](#). First, the hardening variable is added to the local coupled model and the resulting formulation is investigated, where the conditions for the different possible responses are explored. Because of the local treatment, no variational tools are required in this subsection. In the next subsection, as well as in the numeric implementation that follows, the variational approach is illustrated with the nonlocal gradient model that is developed with the addition of the plastic strain gradient term.

The complete material response consists of the following stages:

- (1) An initial elastic phase.
- (2) A homogeneous hardening plastic phase with zero Neumann boundary conditions, or a smooth distribution of plastic strains with zero Dirichlet boundary conditions.

```

1: for  $n = 1$  to  $n_{\text{desp}}$  do
2:   Initialize
3:    $k = 0$ ;
4:   while  $\|\alpha_n^k - \alpha_n^{k-1}\|_{\infty} > \text{tol}_d$  and  $k \leq \text{itmax}$  do
5:     Initialize
6:      $j = 0$ ,  $\Delta d_n^j = \mathbf{0}$ ;
7:     while  $\|R_n^j\|_1 > \text{tol}_p$  and  $k \leq \text{itmax}$  do
8:       Initialize the stiffness matrix and the internal force vector
9:        $K_n^j = \Gamma$ ,  $F_n^{\text{int}^j} = \Gamma$ ;
10:      for  $e = 1$  to  $n_{\text{el}}$  do
11:        Obtain the average damage per element  $\bar{\alpha}$ 
12:        Obtain  $\{\sigma, \epsilon, \epsilon_p, p\}$  via one of the local models, as well as the corresponding tangential
13:        modulus introducing  $E(\bar{\alpha})$  and  $\sigma_y(\bar{\alpha})$ 
14:        Update  $F_n^{\text{int}^j}$  and  $K_n^j$ 
15:      end for
16:      if  $\|R_n^j\|_1 > \text{tol}_p$  then
17:        Obtain the incremental nodal displacements for the next iteration
18:         $\Delta d_n^j = \Delta d_n^j - [K_n^j]^{-1}[R_n^j]$ ;
19:         $j = j + 1$ 
20:      end if
21:    end while
22:    Obtain the nodal damage values  $\alpha$  via (2-11)
23:    if  $\|\alpha_n^k - \alpha_n^{k-1}\|_{\infty} > \text{tol}_d$  then
24:       $k = k + 1$ 
25:    end if
26:  end while
27: end for

```

Algorithm 1. Classical approach elastic-plastic-damage algorithm.

- (3) A coupled plastic-damage phase, with a nonhomogenous distribution of both fields. If Neumann boundary conditions are imposed in the plastic phase, Dirichlet boundary conditions are necessary in the damage field to break the homogeneity of the bar. Each variable will distribute according to its own internal length with a maximum at the center of the bar, with the plastic internal length decreasing as a function of the damage level.
- (4) A localization of the plastic strain evolution at the center of the bar as soon as a threshold level of damage has been reached in the bar.

3.1. Local model with hardening plasticity. In this subsection, the analytical governing equations are presented for the local coupled model. The work carried out is adopted from [Alessi 2013] and the hardening variable is incorporated in the procedure.

3.1.1. General model. The free energy is defined locally as

$$\Psi = \frac{1}{2}E(\alpha)(\epsilon - \epsilon_p)^2 + \frac{1}{2}H(\alpha)p^2, \quad (3-1)$$

where the hardening component has been added to the free energy given by (2-1) for perfect plasticity. A plastic hardening variable $\kappa = |\epsilon_p| = p$ is considered with a plastic modulus $H(\alpha)$. Then, the stress-strain relation becomes

$$\sigma(\epsilon_p, \alpha) = E(\alpha)(\epsilon - \epsilon_p). \quad (3-2)$$

The plasticity yield criterion f_p and the damage criterion f_d read as

$$f_p(\sigma, p, \alpha) = |\sigma| - [\sigma_p(\alpha) + H(\alpha)p] \leq 0, \quad (3-3)$$

$$f_d(\sigma, p, \alpha) = -\frac{1}{2}E'(\alpha)(\epsilon - \epsilon_p)^2 - \frac{1}{2}H'(\alpha)p^2 - \sigma'_p(\alpha)p - w_0 \leq 0, \quad (3-4)$$

where the following properties are defined for each term:

$$E(\alpha) > 0, \quad E'(\alpha) < 0 \forall \alpha \in [0, 1),$$

$$H(\alpha) > 0, \quad H'(\alpha) < 0 \forall \alpha \in [0, 1),$$

$$\sigma_p(\alpha) > 0, \quad \sigma'_p(\alpha) < 0 \forall \alpha \in [0, 1).$$

The local evolution is given by the Kuhn–Tucker conditions and the consistency conditions for each yield surface. Moreover, from (3-3) and (3-4), the yield stresses are

$$\sigma_{yp}(p, \alpha) = \sigma_p(\alpha) + H(\alpha)p, \quad (3-5)$$

$$\sigma_{yd} = \sqrt{\frac{w_0 + \sigma'_p(\alpha)p + 1/2H'(\alpha)p^2}{-1/2E'(\alpha)E(\alpha)^{-2}}}. \quad (3-6)$$

Then, the evaluation of the consistency conditions is required. For this, one uses

$$\dot{f}_p(\sigma, p, \alpha) = E(\alpha)(\dot{\epsilon} - \dot{\epsilon}_p) \text{sign}(\sigma) + (E'(\alpha)(\epsilon - \epsilon_p) - \sigma'_p(\alpha) - H'(\alpha)p)\dot{\alpha} - H(\alpha)\dot{p}, \quad (3-7)$$

$$\begin{aligned} \dot{f}_d(\sigma, p, \alpha) = & E(\alpha)(\dot{\epsilon} - \dot{\epsilon}_p) - (\sigma'_p(\alpha) + H'(\alpha)p)\dot{p} \\ & - \left(\frac{1}{2}E''(\alpha)(\epsilon - \epsilon_p)^2 + \frac{1}{2}H''(\alpha)p^2 + \sigma''_p(\alpha)p \right) \dot{\alpha}. \end{aligned} \quad (3-8)$$

The material response consists of three stages: an elastic phase, a first dissipation phase and a second dissipation phase. These are analyzed next considering increasing monotonic loading.

Elastic phase. An elastic phase is defined by $\sigma < \min(\sigma_{yp}(0, 0), \sigma_{yd}(0, 0))$. The next phase, which begins at a certain stress level, can consist of one of two possible evolutions:

- E-P-*: $\sigma = \sigma_{yp}(0, 0) < \sigma_{yd}(0, 0)$. From the stress-strain relation (3-2), the strain at which the plastic phase begins is

$$\epsilon = \epsilon_{yp} = \sigma_p(0)/E(0).$$

- E-D-*: $\sigma = \sigma_{yd}(0, 0) < \sigma_{yp}(0, 0)$. The damage phase begins at the strain level

$$\epsilon = \epsilon_{yd} = \sqrt{w_0 / -E'(0)}.$$

First dissipation. It begins with $\sigma = \min(\sigma_{yp}(0, 0), \sigma_{yd}(0, 0))$. The two possible evolutions are analyzed:

- E-P-*: ($\epsilon_{yp} \leq \epsilon < \epsilon_{yd}$). Therefore, one has

$$\begin{aligned} \sigma &= \sigma_{yp}(0, 0) < \sigma_{yd}(0, 0), \\ f_p(\sigma, 0, 0) &= 0, \\ f_d(\sigma, 0, 0) &< 0. \end{aligned}$$

For a loading condition, the evolution is obtained through the consistency conditions from (3-7), where

$$\dot{f}_p(\sigma, p, 0) = E(0)(\dot{\epsilon} - \dot{\epsilon}_p) - H(0)\dot{p} = 0.$$

The second dissipation phase begins at the strain level

$$\epsilon = \epsilon_{yd} = \sqrt{\frac{w_0 + \sigma_p'(0)p + 1/2H'(0)p^2}{-1/2E'(0)}} + \epsilon_p.$$

- E-D-*: ($\epsilon_{yd} \leq \epsilon < \epsilon_{yp}$). Therefore, one has

$$\begin{aligned} \sigma &= \sigma_{yd}(0, 0) < \sigma_{yp}(0, 0), \\ f_p(\sigma, 0, 0) &< 0, \\ f_d(\sigma, 0, 0) &= 0, \end{aligned}$$

and the consistency conditions are investigated through (3-8), which yields

$$\dot{f}_d(\sigma, 0, \alpha) = -E'(\alpha)\epsilon\dot{\epsilon} - \frac{1}{2}E''(\alpha)\epsilon^2\dot{\alpha} = 0,$$

which is admissible given $E''(\alpha) > 0$. The second dissipation phase begins at the strain level

$$\epsilon = \epsilon_{yp} = \sigma_p(\alpha) / E(\alpha).$$

Notice that if $\sigma_{yd}(0, \alpha) < \sigma_{yp}(0, \alpha)$ for the entire evolution, this strain level is never reached, resulting in a brittle E-D response.

Second dissipation. Different evolutions can arise, regardless of the first dissipation phase. They are investigated as follows:

- E-*-P: It is required that

$$\begin{aligned} \dot{f}_p(\sigma, p, \alpha) &= E(\alpha)(\dot{\epsilon} - \dot{\epsilon}_p) - H(\alpha)\dot{p} = 0, \\ \dot{f}_d(\sigma, p, \alpha) &= E'(\alpha)(\epsilon - \epsilon_p)\dot{\epsilon} \left(\frac{E(\alpha)}{E(\alpha) + H(\alpha)} - 1 \right) + (-\sigma_p'(\alpha) - H'(\alpha))\dot{p} < 0, \end{aligned} \quad (3-9)$$

which is inadmissible because, given $H(\alpha) > 0$ and $H'(\alpha) < 0$, both the first and second terms are always positive. Therefore, it is impossible for plasticity to evolve by itself once damage has been triggered. It is worth noting that this no longer holds for softening plasticity, where $H(\alpha) < 0$

and $H'(\alpha) > 0$, because the terms in the inequality can eventually become negative. In this work, however, only hardening plasticity is considered.

- **E-*-D:** It is required that

$$\begin{aligned}\dot{f}_p(\sigma, p, \alpha) &= (E'(\alpha)(\epsilon - \epsilon_p) - \sigma'_p(\alpha) - H'(\alpha)p)\dot{\alpha} + E(\alpha)\dot{\epsilon} < 0, \\ \dot{f}_d(\sigma, p, \alpha) &= -E'(\alpha)(\epsilon - \epsilon_p) - \left(\frac{1}{2}E''(\alpha)(\epsilon\epsilon_p)^2 + \frac{1}{2}H''(\alpha)p^2 + \sigma''_p(\alpha)p \right)\dot{\alpha} = 0,\end{aligned}$$

which results in

$$A < -E'(\alpha)(\epsilon - \epsilon_p)/E(\alpha)B, \quad (3-10)$$

where

$$\begin{aligned}A &= \frac{1}{2}E''(\alpha)(\epsilon - \epsilon_p)^2 + \frac{1}{2}H''(\alpha)p^2 + \sigma''_p(\alpha)p > 0, \\ B &= -E'(\alpha)(\epsilon - \epsilon_p) + \sigma'_p(\alpha) + H'(\alpha)p > 0.\end{aligned}$$

Equation (3-10) defines the necessary condition for the evolution of damage without plasticity as the second dissipation phase.

- **E-*-PD:** It is required that

$$\begin{aligned}\dot{f}_p(\sigma, p, \alpha) &= E(\alpha)(\dot{\epsilon} - \dot{\epsilon}_p) + (E'(\alpha)(\epsilon - \epsilon_p) - \sigma'_p(\alpha) - H'(\alpha)p)\dot{\alpha} - H(\alpha)\dot{p} = 0, \\ \dot{f}_d(\sigma, p, \alpha) &= -E'(\alpha)(\epsilon - \epsilon_p) - (\sigma'_p(\alpha) + H'(\alpha)p)\dot{p} \\ &\quad - \left(\frac{1}{2}E''(\alpha)(\epsilon\epsilon_p)^2 + \frac{1}{2}H''(\alpha)p^2 + \sigma''_p(\alpha)p \right)\dot{\alpha} = 0,\end{aligned}$$

which results in

$$-E'(\alpha)(\epsilon - \epsilon_p)/E(\alpha)B < A, \quad (3-11)$$

defining the necessary condition for the coupled plastic-damage second dissipation phase.

3.1.2. Specific model. We focus on the E-P-PD evolution. Recalling (2-9) from the classical approach, the constitutive functions

$$E(\alpha) = E_0(1 - \alpha)^2, \quad H(\alpha) = H_0(1 - \alpha)^2, \quad \sigma_p(\alpha) = \sigma_{p_0}(1 - \alpha)^2, \quad (3-12)$$

are used. where the constitutive function of the plastic modulus has been added, with H_0 as the initial plastic modulus. Then, the yield stresses become

$$\sigma_{yp}(p, \alpha) = (1 - \alpha)^2(\sigma_{p_0} + H_0p), \quad (3-13)$$

$$\sigma_{yd}(p, \alpha) = \sqrt{(w_0 - (2\sigma_{p_0}p + H_0p^2)(1 - \alpha))E_0(1 - \alpha)^3}. \quad (3-14)$$

Both dissipation phases are analyzed:

- **First dissipation:** From (3-13) and (3-14), the yield stresses become

$$\begin{aligned}\sigma_{yp}(0, 0) &= \sigma_{p_0}, \\ \sigma_{yd}(0, 0) &= \sqrt{w_0E_0}.\end{aligned}$$

Therefore, if $\sigma_{p_0} < \sqrt{w_0 E_0}$ holds, a plasticity phase is ensured as the first dissipation.

- Second dissipation: With nonsoftening plasticity as the first dissipation phase, a second dissipation is phase is guaranteed. Recalling that for monotonic loading $p = \epsilon_p$, the yield strain is

$$\epsilon_{yd} = \sqrt{\frac{w_0 - 2\sigma_{p_0} p_{yd} - H_0 p_{yd}^2}{E_0}} + p_{yd}, \quad (3-15)$$

where p_{yd} is the accumulated plastic strain corresponding to ϵ_{yd} . A coupled response needs to be assured, for which $\sigma_{yd}(p_{yd}, \alpha) > \sigma_{yp}(p, \alpha)$ needs to be verified during the evolution. Using the stress-strain relation (3-2), (3-15) and (3-13) one has

$$\sqrt{\frac{w_0 - 2\sigma_{p_0} p_{yd} - H_0 p_{yd}^2}{E_0}} - \frac{\sigma_{p_0} + H_0 p_{yd}}{E_0} = 0,$$

which results in

$$(H_0^2/E_0 + H_0) p_{yd}^2 + (\sigma_{p_0} H_0/E_0 + 2\sigma_{p_0}) p_{yd} + (\sigma_{p_0}^2/E_0 - w_0) = 0.$$

With this, the value $p = p_{yd}$ is given and from equations (3-13) and (3-14), $\sigma_{yd}(p_{yd}, \alpha) > \sigma_{yp}(p, \alpha)$ must hold for a coupled evolution.

Finally, the complete evolution is explicitly given by:

- Elastic phase: $\epsilon \in [0, \epsilon_{yp})$.

$$p(t) = 0, \quad \alpha(t) = 0, \quad \sigma(t) = E_0 \epsilon.$$

- Plastic phase: $\epsilon \in [\epsilon_{yp}, \epsilon_{yd})$.

$$p(t) = (\epsilon E_0 - \sigma_{p_0}) / (E_0 + H_0), \quad \alpha(t) = 0, \quad \sigma(t) = \sigma_{p_0} + H_0 p.$$

- Plastic-damage phase: $\epsilon \in [\epsilon_{yd}, \infty)$.

$$p(t) = \frac{\epsilon E_0 - \sigma_{p_0}}{E_0 + H_0}, \quad \alpha(t) = 1 - \frac{w_0}{E_0(\epsilon - p)^2 + H_0 p^2 + 2\sigma_{p_0} p}, \quad \sigma(t) = (\sigma_{p_0} + H_0 p) (1 - \alpha)^2.$$

Energy dissipation. From the Clausius–Duhem inequality, one has

$$\sigma \dot{\epsilon} - \dot{\Psi} \geq 0,$$

from where

$$\left(-\frac{1}{2} E'(\alpha) (\epsilon - \epsilon_p)^2 - \frac{1}{2} H'(\alpha) p^2 \right) \dot{\alpha} + \sigma \dot{\epsilon}_p - H(\alpha) p \dot{p} \geq 0.$$

The plastic dissipation reads as

$$\begin{aligned} \Phi_p &= \sigma \dot{\epsilon}_p - H(\alpha) p \dot{p} \\ &= \dot{p} [|\sigma| - H(\alpha) p] \\ &= (\sigma_p(\alpha)) \dot{p} \geq 0, \end{aligned} \quad (3-16)$$

whereas the damage dissipation is

$$\begin{aligned}\Phi_d &= \left(-\frac{1}{2}E'(\alpha)(\epsilon - \epsilon_p)^2 - \frac{1}{2}H'(\alpha)p^2 \right) \dot{\alpha} \\ &= (\sigma_p'(\alpha) + w_0)\dot{\alpha} \geq 0.\end{aligned}\quad (3-17)$$

3.2. Global gradient model.

3.2.1. Energy functional. The nonlocal model is developed with a variational treatment. First, the energy potentials have to be defined. The stored elastic energy $\mathcal{E} = \int_0^L \Psi dx$ is given by

$$\mathcal{E}(u, \epsilon_p, p, \alpha) = \int_0^L \frac{1}{2}E(\alpha)(u' - \epsilon_p)^2 + \frac{1}{2}H(\alpha)p^2 dx, \quad (3-18)$$

where the hardening term is considered. From (3-16) and (3-17), the total dissipation potential is defined as

$$\begin{aligned}\Phi(p, \alpha, p', \alpha', \dot{p}, \dot{\alpha}, \dot{p}', \dot{\alpha}') &= \Phi_p + \partial_t \left(\frac{1}{2}\eta_p(\alpha)^2 p'^2 \right) + \Phi_d + \partial_t \left(\frac{1}{2}\eta_d^2 \alpha'^2 \right) \\ &= (\sigma_p(\alpha))\dot{p} + \partial_t \left(\frac{1}{2}\eta_p(\alpha)^2 p'^2 \right) + w_0\dot{\alpha} + \sigma_p'(\alpha)\dot{\alpha} + \partial_t \left(\frac{1}{2}\eta_d^2 \alpha'^2 \right),\end{aligned}\quad (3-19)$$

where the terms corresponding to the plastic strain gradient and the damage gradient have been added, with $\eta_p(\alpha)$ as a variable internal length scale. The damage gradient term is kept to avoid an abrupt damage localization and an instantaneous rupture as soon as damage is triggered. With (3-19), the dissipated work \mathcal{D} is defined as

$$\begin{aligned}\mathcal{D}(u, \epsilon_p, p, \alpha) &= \int_0^L \frac{1}{2}E(\alpha)(u' - \epsilon_p)^2 + \frac{1}{2}H(\alpha)p^2 dx \\ &\quad + \int_0^L \sigma_y(\alpha)p + \frac{1}{2}\eta_p(\alpha)^2 p'^2 dx + \int_0^L w_0\alpha + \frac{1}{2}\eta_d^2 \alpha'^2 dx.\end{aligned}\quad (3-20)$$

The energy functional is defined with (3-20) and (3-18) as

$$\begin{aligned}\mathcal{W}(u, p, \alpha) &= \mathcal{E}(u, p, \alpha) + \mathcal{D}(u, p, \alpha) \\ &= \int_0^L \frac{1}{2}E(\alpha)(u' - \epsilon_p)^2 + \frac{1}{2}H(\alpha)p^2 dx \\ &\quad + \int_0^L \sigma_p(\alpha)p + \frac{1}{2}\eta_p(\alpha)^2 p'^2 dx + \int_0^L w_0\alpha + \frac{1}{2}\eta_d^2 \alpha'^2 dx.\end{aligned}\quad (3-21)$$

3.2.2. Energetic formulation. The building blocks of the variational energetic formulation are the following conditions:

- (1) Stability condition.
- (2) Energy balance.
- (3) Irreversibility condition.

The irreversibility condition is imposed on the damage variable and is given by (2-10). This condition is applied numerically by simply considering the damage value corresponding to the previous load step as the minimum level of damage for each corresponding node as

$$\alpha_n^i = \begin{cases} \alpha_n^i, & \text{if } \alpha_n^i \geq \alpha_{n-1}^i, \\ \alpha_{n-1}^i, & \text{if } \alpha_n^i < \alpha_{n-1}^i, \end{cases} \quad (3-22)$$

where α_n^i is the damage value for the n -th load step and the i -th node. The other two conditions are explored in this section. From now on, only monotonic loading is considered, for which $\epsilon_p = p$.

Stability condition. By differentiating potentials (3-18) and (3-20), the first order stability condition yields

$$\begin{aligned} \mathcal{W}(u, p, \alpha)(\tilde{u}, \tilde{p}, \tilde{\alpha}) &= \mathcal{E}'(u, p, \alpha) + \mathcal{D}'(u, p, \alpha) \\ &= \int_0^L E(\alpha)(u' - p)\tilde{u}' + (-E(\alpha)(u' - p) + \sigma_p(\alpha) + H(\alpha)p)\tilde{p} + \eta_p(\alpha)^2 p' \tilde{p}' \\ &\quad + \left(\frac{1}{2} E'(\alpha)(u' - p)^2 + \frac{1}{2} H'(\alpha)p^2 + \sigma_p'(\alpha)p + w_0 + \eta_p(\alpha)\eta_p'(\alpha)p'^2 \right) \tilde{\alpha} + \eta_d^2 \alpha' \tilde{\alpha}' dx \geq 0, \end{aligned}$$

from where the following cases are analyzed:

- For $\tilde{p} = \tilde{\alpha} = 0$,

$$\int_0^L E(\alpha)(u' - p)\tilde{u}' dx = 0, \quad (3-23)$$

which is the weak form of the equilibrium equation in the absence of external loads.

- For $\tilde{u} = \tilde{\alpha} = 0$,

$$\int_0^L \left((-E(\alpha)(u' - p) + \sigma_p(\alpha) + H(\alpha)p)\tilde{p} + \eta_p(\alpha)^2 p' \tilde{p}' \right) dx \geq 0, \quad (3-24)$$

which is the weak form of the plasticity yield criterion. After integrating the last term by parts, the gradient-dependent yield criterion is recovered in the local form

$$f_p(u, p, \alpha) = \sigma - [\sigma_p(\alpha) + H(\alpha)p] + \eta_p(\alpha)^2 p'' \leq 0. \quad (3-25)$$

- For $\tilde{u} = \tilde{p} = 0$,

$$\int_0^L \left(\frac{1}{2} E'(\alpha)(u' - p)^2 + \sigma_p'(\alpha)p + \frac{1}{2} H'(\alpha)p^2 + w_0 + \eta_p(\alpha)\eta_p'(\alpha)p'^2 \right) \tilde{\alpha} + \eta_d^2 \alpha' \tilde{\alpha}' dx \geq 0, \quad (3-26)$$

obtaining the weak form of the damage criterion. Again, the last term is integrated by parts and the gradient-dependent yield criterion is recovered in the local form

$$f_d(u, p, \alpha) = -\frac{1}{2} E'(\alpha)(u' - p)^2 - \sigma_p'(\alpha)p - \frac{1}{2} H'(\alpha)p^2 - w_0 - \eta_p(\alpha)\eta_p'(\alpha)p'^2 + \eta_d^2 \alpha'' \leq 0, \quad (3-27)$$

where the damage gradient term is observed. Also, the plastic gradient term is present due to the possible coupling of the plastic internal length to the damage variable. This problem will be treated once the constitutive functions are introduced.

Energy balance. A procedure analogous to the treatment of the stability condition is carried out. The energy balance leads to

$$\int_0^L -E(\alpha)(u' - p)\dot{u}' + (E(\alpha)(u' - p) - \sigma_p(\alpha) - H(\alpha) + \eta_p(\alpha)p'')\dot{p} + \left(-\frac{1}{2}E'(\alpha)(u' - p)^2 - \frac{1}{2}H'(\alpha)p^2 - \sigma_p'(\alpha)p - w_0 - \eta_p(\alpha)\eta_p'(\alpha)p'^2 + \eta_d\alpha''\right)\dot{\alpha} dx = 0. \quad (3-28)$$

The following cases are analyzed:

- For $\dot{u} = \dot{\alpha} = 0$, using (3-25), the plasticity consistency conditions are obtained as

$$f_p(u, p, \alpha)\dot{p} = 0.$$

- For $\dot{u} = \dot{p} = 0$, using (3-27), the damage consistency conditions are obtained as

$$f_d(u, p, \alpha)\dot{\alpha} = 0.$$

3.2.3. Alternate minimization. The finite element resolution that is applied in this work is shown in this subsection. All the integrals, when necessary, are solved through Gaussian quadrature. To gain precision and a more accurate response, no average values are taken, and the state variables are approximated as follows:

- The displacement field is approximated with quadratic shape functions and three-node elements.
- Both the plastic strain field and the damage field are approximated with linear shape functions and two-node elements.

The same constitutive functions (Equation (3-12))

$$E(\alpha) = E_0(1 - \alpha)^2, \quad H(\alpha) = H_0(1 - \alpha)^2, \quad \sigma_p(\alpha) = \sigma_{p_0}(1 - \alpha)^2,$$

are applied. Additionally, the plastic internal length is taken as

$$\eta_p(\alpha) = \begin{cases} \eta_{p_0}(\beta - \max(\alpha)), & \text{if } \max(\alpha) \leq \beta \\ 0, & \text{if } \max(\alpha) > \beta \end{cases},$$

where η_{p_0} is the initial internal length, $\beta \in [0, 1]$ is a threshold level of damage and $\max(\alpha)$ is the maximum value of damage, which will be located at the center of the bar. This choice of function for the plastic internal length avoids the dependence of the damage variable on the plastic strain gradient because the term $\eta_p(\alpha)\eta_p'(\alpha)p'^2$ disappears from the damage criterion.

The alternate minimization follows:

- Minimization with respect to the displacement field $\mathcal{W}(u, \epsilon_p, \alpha)(\tilde{u}, 0, 0)=0$,

$$\left. \frac{d}{dh} \mathcal{W}(u + h\tilde{u}, \epsilon_p, \alpha) \right|_{h=0} = (3-23).$$

Introducing the constitutive functions, approximation functions and shape functions, the matrix form is obtained as

$$\int_0^L E_0(1 - N\alpha_e)^2 \mathbf{M}'^T \mathbf{M}' dx \mathbf{u} - \int_0^L E_0(1 - N\alpha)^2 \mathbf{M}'^T N dx \mathbf{p} = 0, \quad (3-29)$$

where \mathbf{M} and N are the shape functions of three-node elements and two-node elements, respectively.

- Minimization with respect to the plastic strain $\mathcal{W}'(u, \epsilon_p, \alpha)(0, \tilde{\epsilon}_p, 0) = 0$,

$$\left. \frac{d}{dh} \mathcal{W}(u, \epsilon_p + h\tilde{\epsilon}_p, \alpha) \right|_{h=0} = (3-24).$$

Along with the constitutive functions, the matrix form is

$$\begin{aligned} \int_0^L -E_0(1 - N\alpha)^2 N^T \mathbf{M}' dx \mathbf{u} + \int_0^L E_0(1 - N\alpha)^2 N^T N dx \mathbf{p} \\ + \int_0^L \sigma_{p0}(1 - N\alpha)^2 N^T dx + \int_{\Omega} H_0(1 - N\alpha)^2 N^T N dx \mathbf{p} \\ + \int_0^L H(\beta - \max(\alpha)) \eta_{p0}^2 (\beta - \max(\alpha))^2 N'^T N' dx \mathbf{p} = 0, \end{aligned} \quad (3-30)$$

where H is the Heaviside step function.

- Minimization with respect to the damage field $\mathcal{W}'(u, \epsilon_p, \alpha)(0, 0, \tilde{\alpha}) = 0$,

$$\left. \frac{d}{dh} \mathcal{W}(u, \epsilon_p, \alpha + h\tilde{\alpha}) \right|_{h=0} = (3-26).$$

Again, the corresponding matrix form is obtained as

$$\int_0^L (w_0 - R) N^T dx + \int_{\Omega} R N^T N dx \alpha + \int_{\Omega} \eta_d^2 N'^T N' dx \alpha, \quad (3-31)$$

where

$$R = E_0(\mathbf{M}'\mathbf{u} - N\mathbf{p})^2 + 2\sigma_{p0}N\mathbf{p} + H_0N\mathbf{p}N\mathbf{p}. \quad (3-32)$$

The local vector forms are solved and the global vectors are found for each variable alternatively.

3.3. Computational implementation. The numeric implementation leads to the *alternate minimization algorithm*. The main characteristics are:

- The displacements are imposed gradually.
- The trial elastic state is given to all the elements by verifying equilibrium and finding the elastic displacement distribution.
- The plastic state is recovered by finding the global plastic strain vector.
- The plastic-damage field is finally obtained by finding the global damage vector.
- Three convergence criteria are applied: L_2 norms for the displacement field and the plastic strain field, with tolerances tol_u and tol_p , respectively, and L_{∞} norm for the damage field with tolerance tol_d .

The computational process is summarized in [Algorithm 2](#).

```

1: for  $n = 1$  to  $n_{\text{desp}}$  do
2:   Initialize
    $k = 0$ ;
3:   while ( $\|u_n^k - u_n^{k-1}\|_2 > \text{tol}_u$  or  $\|\epsilon_{p_n}^k - \epsilon_{p_n}^{k-1}\|_2 > \text{tol}_p$  or  $\|\alpha_n^k - \alpha_n^{k-1}\|_\infty > \text{tol}_d$ ) and  $k \leq \text{itmax}$ 
   do
4:      $k = k + 1$ ;
5:     Obtain  $u_n^k = \text{argmin}_u \mathcal{W}(u, \epsilon_{p_n}^{k-1}, p_n^{k-1}, \alpha_n^{k-1})$  from the solution of (3-29)
6:     Obtain  $\epsilon_{p_n}^k, p_n^k = \text{argmin}_{\epsilon_p} \mathcal{W}(u_n^k, \epsilon_p, p, \alpha_n^{k-1})$  from the solution of (3-30)
7:     Obtain  $\alpha_n^k = \text{argmin}_\alpha \mathcal{W}(u_n^k, \epsilon_{p_n}^k, p_n^k, \alpha)$  from the solution of (3-31) and apply the irreversibility
   condition with (3-22)
8:   end while
9: end for

```

Algorithm 2. Energetic formulation of the *alternate minimization algorithm*.

4. Numerical simulations

The results of the numerical simulations are explored in this section. First, the classical approach is analyzed. The evolution of the state variables for the viscoplastic model is first illustrated. Then, the tendency of the model towards the perfect plasticity variational model as the loading rate tends to zero is shown. The variational approach follows. The evolution of the local hardening plasticity and gradient damage model is first analyzed, and the results are, on some level, compared to the viscoplastic model. Then, the evolution of the state variables for the gradient plasticity and gradient damage model is shown and the main characteristics are described.

4.1. Classical model. As mentioned, the local classical approach provides a response where the strains localize in the plastic phase in the element where the displacements are imposed. This problem is solved by introducing rate-dependence in the plastic phase, by means of the viscoplastic model. Although this model is used to represent the response of materials that exhibit rate-dependence, it can be demonstrated that as the ratio $\Delta t/v \rightarrow \infty$, the viscoplastic response tends towards the rate-independent plastic model [Simo and Hughes 1998]. For the definition of the numerical model, the loading rate $v = \Delta u/\Delta t$ is introduced as the parameter used to control the rate-dependence effect that viscosity introduces in the model, given that $\Delta t/v \rightarrow \infty$ and $v \rightarrow 0$ are equivalent conditions. The constitutive parameters used in the simulations are in Table 1 and the results of the viscoplastic evolution are illustrated in Figures 1 and 2. In Figure 1 (left), the stress-displacement curve is shown. Two main phases in the material response can be observed, corresponding to the perfect plasticity phase and the plasticity-damage phase. The displacement profile shown in Figure 1 (right) shows an initially smooth evolution, leading to a jump in the displacement field as damage evolves. In Figure 2 (left) the plastic deformation profiles are shown. During the plasticity phase, the plastic deformations evolve uniformly over the bar, but after damage is triggered, the region in which plasticity evolves reduces continuously, until it concentrates in one or two elements in the middle of the bar. The size of this region is controlled by the value of the loading rate, as seen in Figure 4 (left). This behavior has been observed before in [Niazi et al. 2013; Needleman 1988], and has been attributed to an implicit internal length included in the viscoplastic regularization.

	E_0 (MPa)	σ_{y_0} (MPa)	H_0 (MPa)	η_d (MPa ^{1/2} · m)	η_p (MPa ^{1/2} · m)	ν (MPa · s)	w_0 (MPa)	β
classical viscoplasticity	71300	345	–	0.55	–	25	30	–
local hardening plasticity	71300	345	5000	0.80	–	–	30	–
grad. dependent plasticity	71300	345	250	0.55	10	–	30	0.85

Table 1. Constitutive parameters used in the simulations.

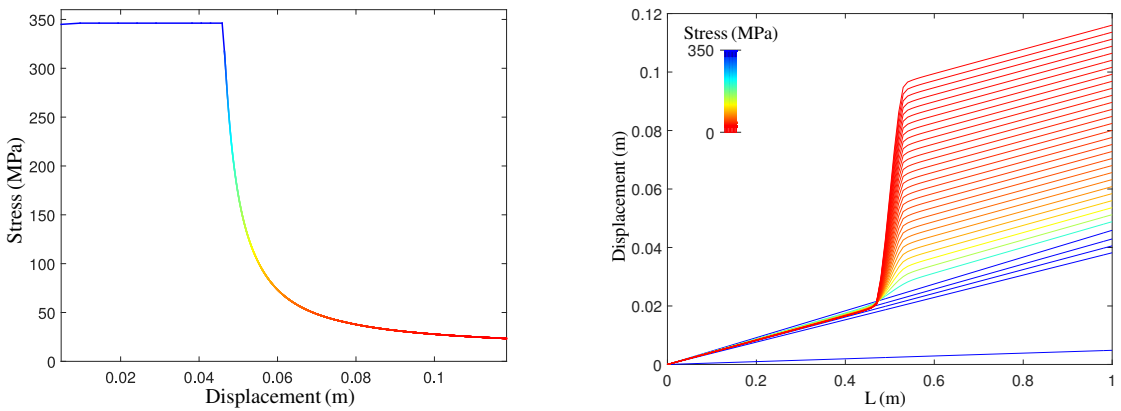


Figure 1. Stress-displacement curve (left) and displacement profiles (right) for the evolution of the classical viscoplastic and gradient damage model with 100 elements.

The damage profile observed in [Figure 2](#) (right) shows an initially smooth distribution. As damage evolves, the spatial distribution tends to an abrupt jump in the spatial derivative of damage in the center of the bar. Another interesting result of the model is length in which the damage and plastic deformation profiles evolve during the loading process. Material damage continuously diffuses along the bar during the evolution, allowing the model to represent void coalescence during material failure. On the other hand, the size of the zone in which the plastic deformations evolve is gradually reduced, allowing the concentration of deformations at the center of the bar. This, along with the jump in the displacement field, represents the formation of a cohesive crack.

The viscoplastic model is shown to converge to the variational model in [\[Alessi 2013\]](#) as the loading rate tends to zero. This can be observed in [Figures 3 and 4](#) for different loading rates $v = \Delta u / \Delta t$. In [Figure 3](#) (left), it can be observed how the stress in the bar increases as the loading rate increases, as expected because of the hardening effect of viscoplasticity.

Additionally, a numerical disadvantage of the classical model is observed in the capacity of the algorithm to converge. For a determined loading rate, the steps at which the displacements are imposed can be too large, causing nonconvergence. Specifically, the total energy never reaches a minimum and oscillates between iterations. This effect is shown for a nonconvergence simulation in [Figure 5](#).

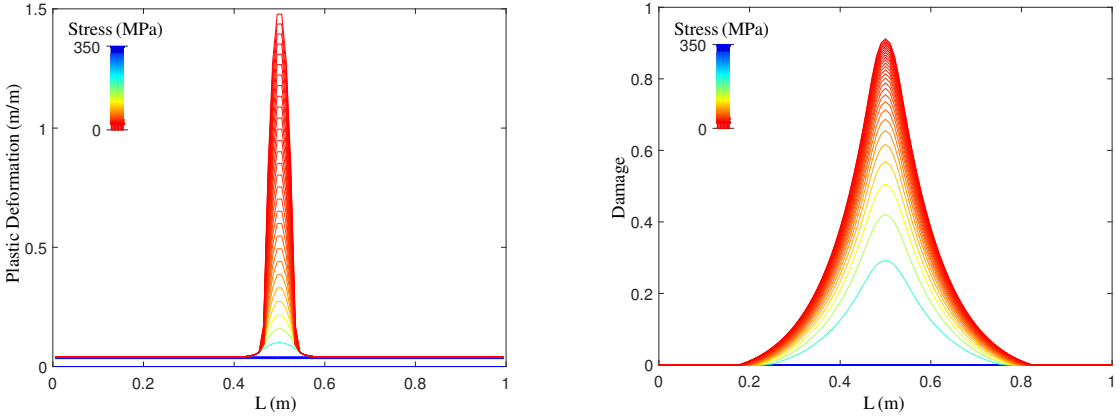


Figure 2. Plastic strain (left) and damage profiles (right) for the evolution of the classical viscoplastic and gradient damage model with 100 elements.

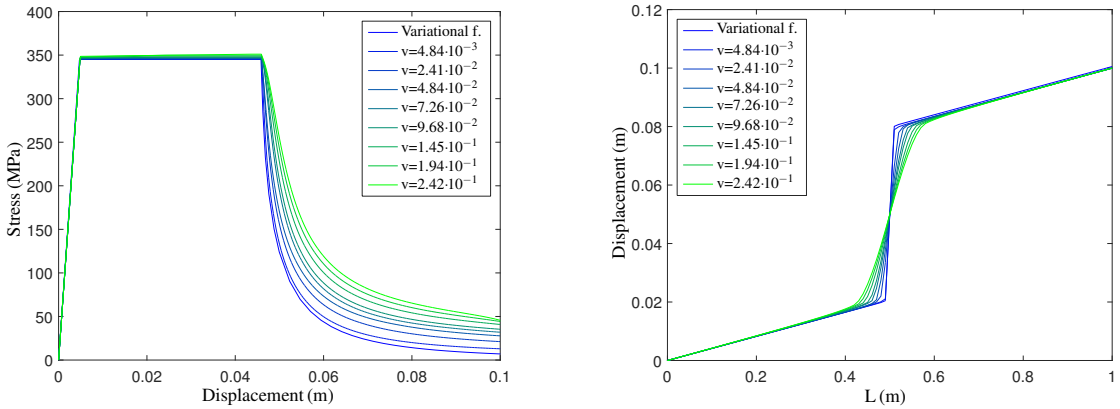


Figure 3. Stress-displacement curves (left) and displacement profiles (right) for the classical viscoplastic model using different loading rates and compared to the variational with 100 elements.

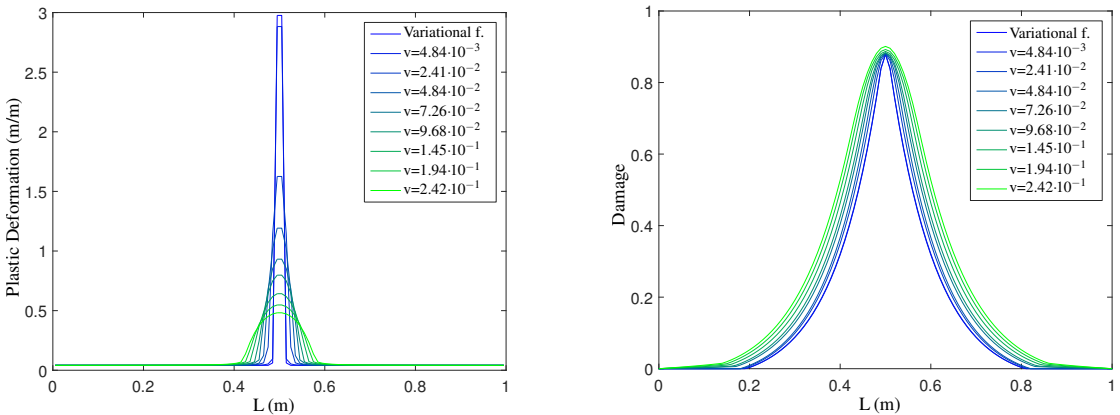


Figure 4. Plastic strain (left) and damage profiles (right) for the classical viscoplastic model using different loading rates and compared to the variational model with 100 elements.

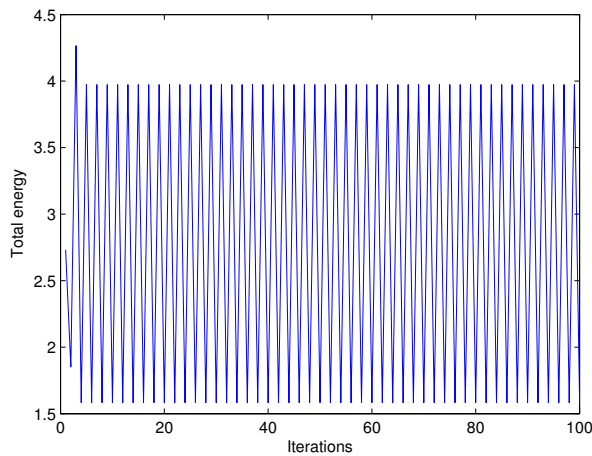


Figure 5. Nonconvergence of the classical approach.

4.2. Variational model.

4.2.1. Hardening plasticity and gradient damage. The results of the simulations of local hardening plasticity and gradient damage are illustrated. The constitutive parameters that were used are shown in Table 1.

The main feature of the local plasticity model can be appreciated in the evolution of the plastic strains shown in Figure 6. There is an initial implicit internal length caused by the hardening variable, and the evolution eventually narrows and concentrates at the center of the bar.

In Figure 7 (left), the displacement profile shows a relatively smooth evolution as the plastic modulus increases. This result is similar to the effect of increasing the loading rate in the viscoplastic model because in both cases, the material becomes stiffer. Also, the plastic strain profile shown in Figure 7

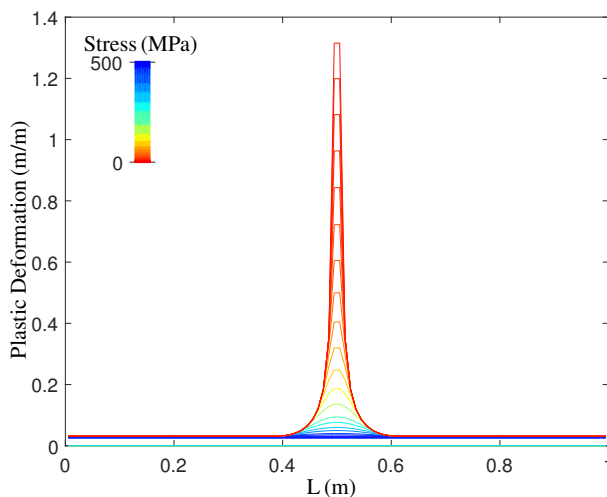


Figure 6. Plastic strain profile for the variational hardening plasticity and gradient damage model with 100 elements.

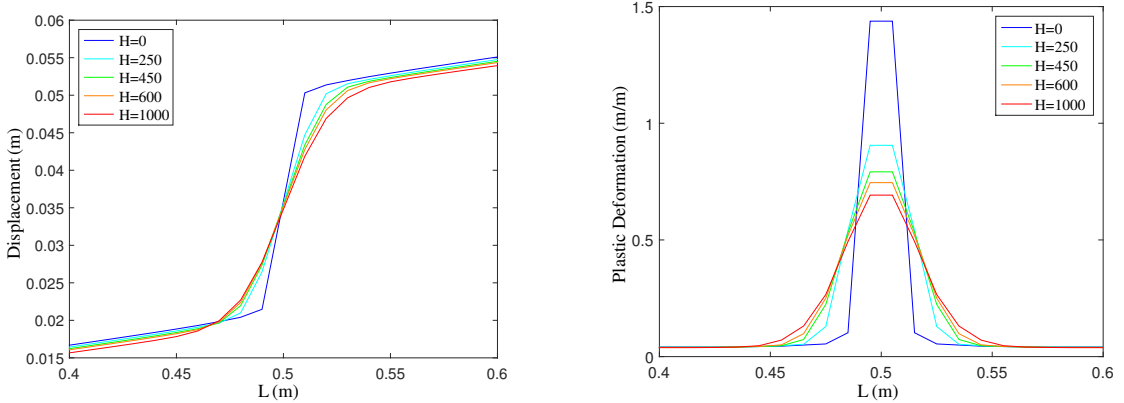


Figure 7. Displacement (left) and plastic strain profiles (right) for the variational hardening plasticity and gradient damage model, varying the hardening modulus with 100 elements.

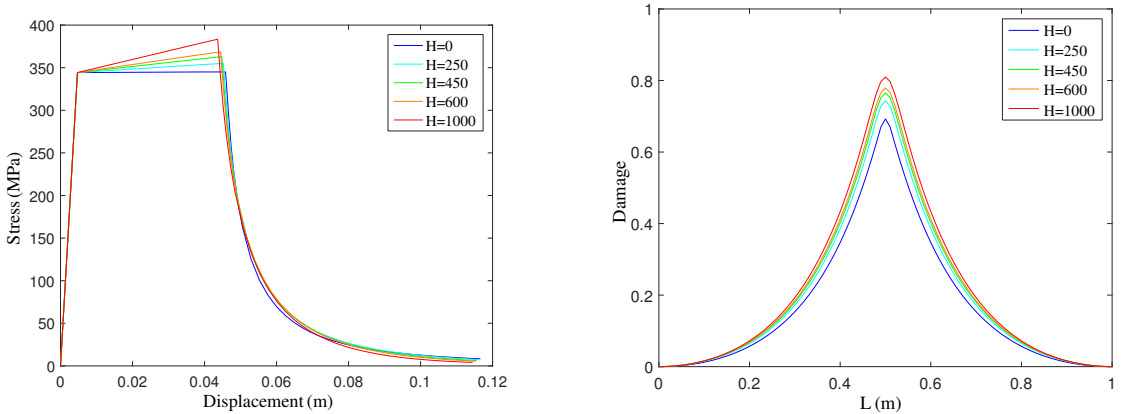


Figure 8. Stress-displacement curves (left) and damage profiles (right) for the variational hardening plasticity and gradient damage model, varying the hardening modulus with 100 elements.

(right) shows that the plastic strains concentrate more and are higher as the plastic modulus decreases. Clearly, $H = 0$ results in the central concentration, recovering the perfect plasticity model in [Alessi 2013]. This result also resembles the plastic strain distribution of the viscoplastic model as the loading rates decrease.

The increase of stress in the plastic phase results in an earlier activation of damage when compared to both the perfect plasticity model and the viscoplastic model, where the damage is triggered at the same strain level. This result is shown in the damage yield points of Figure 8 (left). Clearly, the damage yield stress is reached early for higher values of H . Additionally, Figure 8 (right) shows that the damage response is significantly sensitive with respect to the hardening variable. Because of this coupled evolution, the stress drops to zero at a higher rate as the plastic modulus increases, as shown in the damage phase of Figure 8 (left). Physically, this result can be interpreted as the simulation of a material behavior where hardening also implicates less ductility and a higher loss of stiffness in the softening regime.

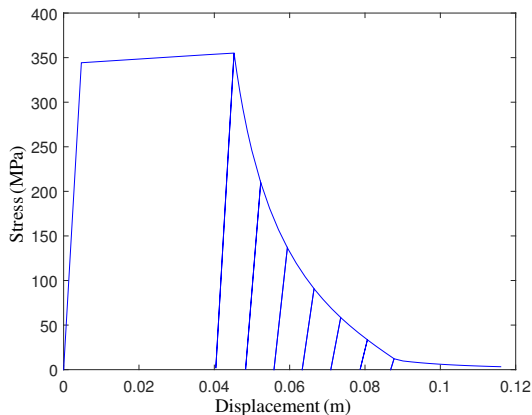


Figure 9. Unloading paths for the gradient plasticity and gradient damage model with 101 elements.

4.2.2. Complete gradient model. The results of the simulations of the complete gradient model are presented. The constant values that were used are shown in Table 1. Because of the nodal distribution of the plastic strains, three nodal elements are considered with quadratic approximations on the displacement field.

Figure 9 shows the unloading paths, where the loss of stiffness can be observed in the damage phase. In Figure 10 (left), the stress-displacement curve is shown in relation to the evolution of the state variables. The results are almost identical to the local hardening model with the exception of the damage phase, where initially the stress drops at a slightly slower rate. Once the damage level has reached the threshold value, the local plasticity tendency is recovered. Both the displacement profile of Figure 10 (right) and the damage profile of Figure 11 (right) also show similar results, presenting initially smooth spatial distributions. The response can be compared to the results of viscoplastic model for relatively high loading rates. On the other hand, the plastic strain profile shown in Figure 11 (left) highlights the main features of the variable plastic strain gradient term. The evolution begins with a wider localization zone then the local plasticity model for the same plastic modulus due to the effect of the gradient term. Then,

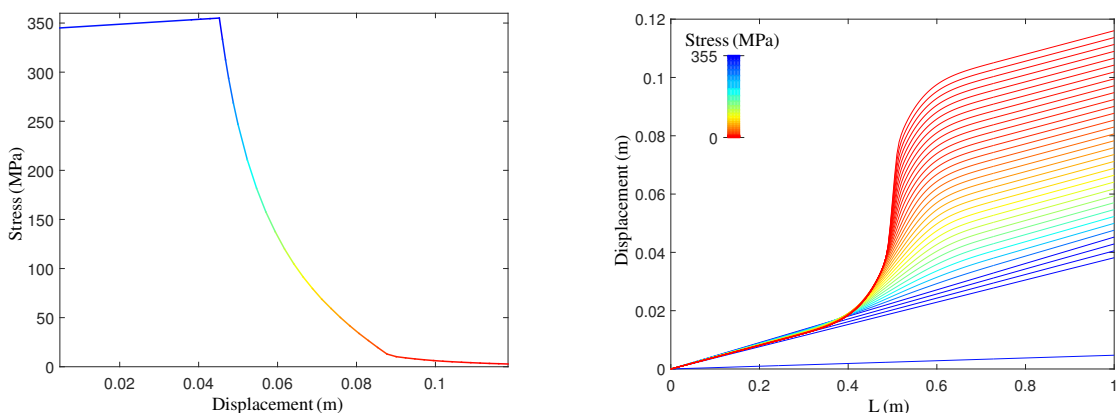


Figure 10. Stress-displacement curve (left) and displacement profile (right) for the evolution of the variational gradient plasticity and gradient damage model with 101 elements.

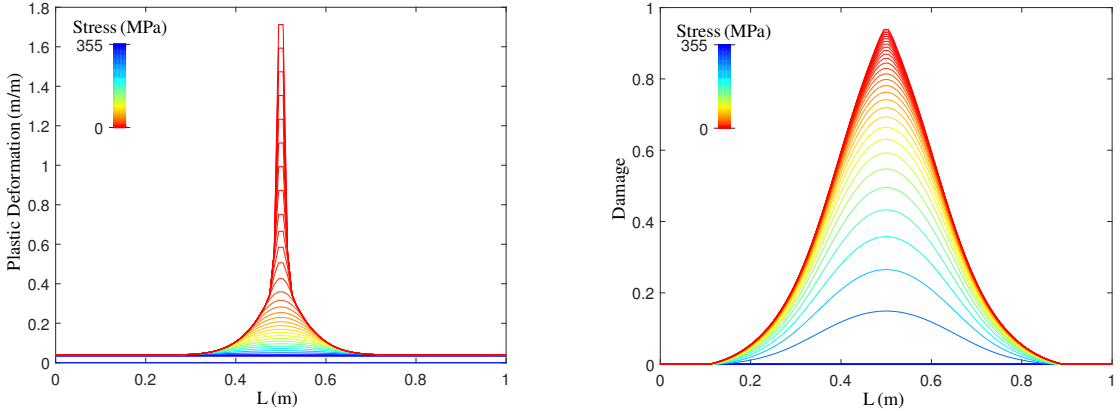


Figure 11. Plastic strain (left) and damage profiles (right) for the evolution of the variational gradient plasticity and gradient damage model with 101 elements.

the damage threshold value is reached and the evolution concentrates in the center of the bar, thereby representing the cohesive crack. Clearly, one of the advantages of this model is that the initial localization region can be controlled without changing the plastic modulus or introducing rate-dependence, which are constant properties of the material.

The energy contributions for the evolution are shown in Figure 12. It is evident that as the stored elastic energy (composed of elastic energy and plastic energy) tends to zero, the total energy becomes a sum of the different contributions of dissipative energies. The total dissipative energy of the bar evolves in the localization zone.

Figures 13 and 14 show the mesh-dependence of the model. Even for a very coarse mesh (11 elements), the tendency is well represented. Clearly, there is low sensitivity to the mesh size, and the plastic strain

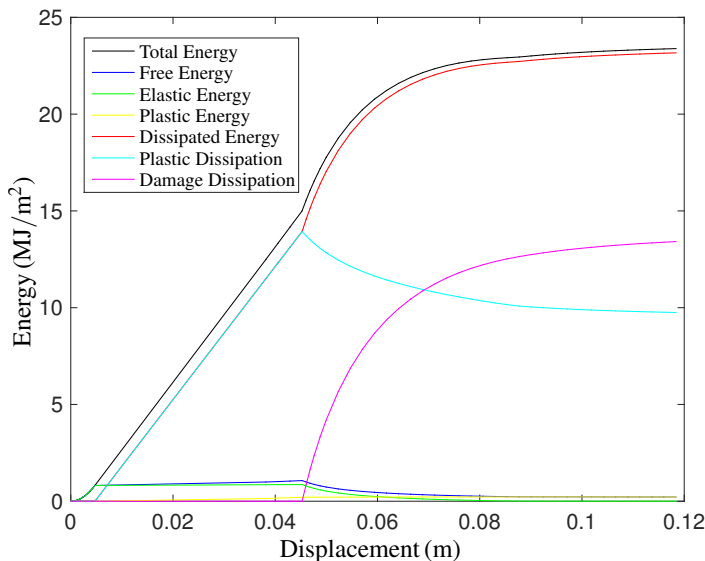


Figure 12. Energy contributions for the variational gradient plasticity and gradient damage model.

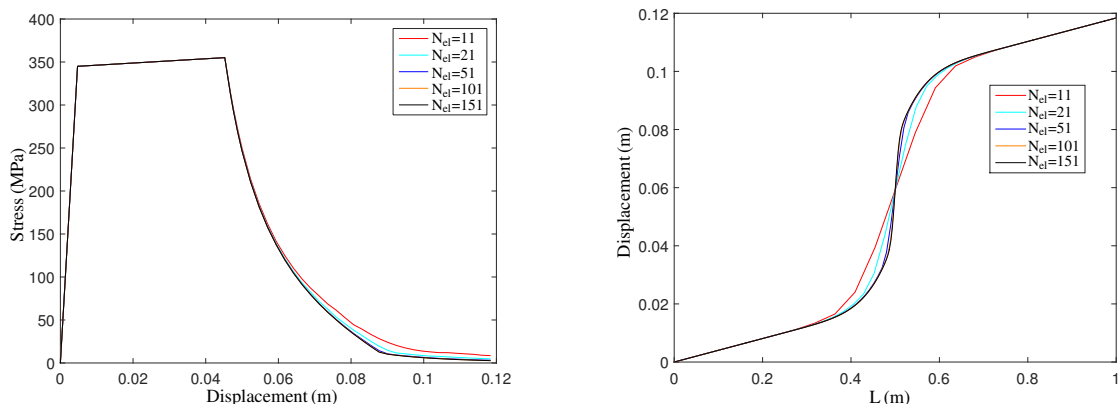


Figure 13. Stress-displacement curve (left) and displacement profiles (right) for the variational gradient plasticity and gradient damage model for different mesh sizes.

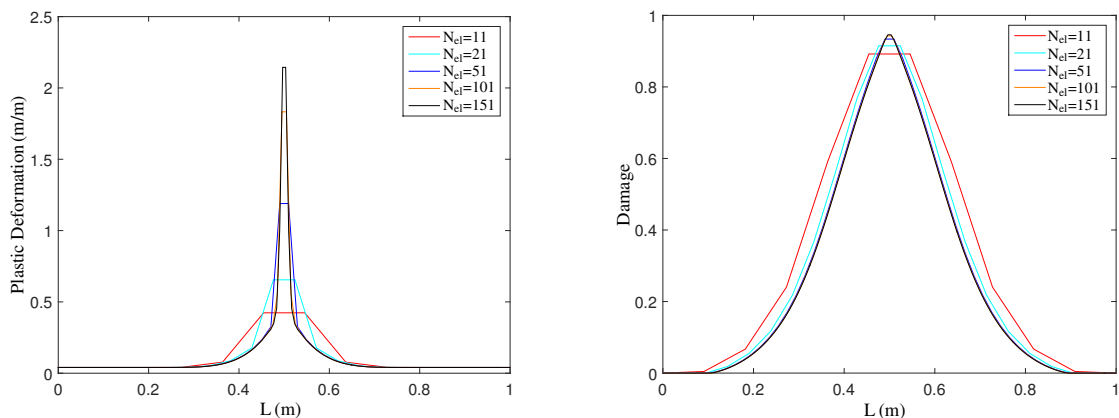


Figure 14. Plastic strain (left) and damage profiles (right) for the variational gradient plasticity and gradient damage model for different mesh sizes.

profiles show that as the mesh size decreases, the concentration of the plastic strains eventually tend to the Dirac delta, as described in [Alessi 2013].

5. Conclusions and perspectives

In this work, the behavior of nonlocal regularized plastic-damage models, in both classical and variational settings has been explored. In the classical approach, the local viscoplastic regularization was used, resulting in the introduction of an implicit internal length in the model, where the size of the localization zone is reduced during the loading process. This is triggered in the plasticity-damage phase and can be controlled through the loading rate. This feature allowed the model to represent a very interesting behavior of the plastic strain spatial distribution and evolution during the final stage of damage and beginning of fracture.

On the other hand, the variational approach in [Alessi 2013] was enriched to include hardening as well as an explicit internal length to control the size of the plastic strain localization zone. The local

evolution was investigated via the consistency conditions, and the addition of the hardening variable furnishes an interesting result, namely (3-9). Clearly, a negative value of the plastic modulus can result in softening behavior without loss of stiffness, even if damage was triggered before. Thus, condition (3-9) should be met for a physically appropriate response. In the numerical simulations, only hardening was considered. As we saw, the hardening variable introduced an implicit internal length that decreases with further loading in the plastic deformation profile, where the initial size of the localization is controlled by the plastic modulus. Similar to the viscoplastic model, the implicit internal length distributes the plastic strains in a certain region; however, the spatial distribution eventually narrows, appropriately representing a jump in the displacement field. Building over this, an explicit internal length was introduced by means of the plastic strain gradient. Taking advantage of the one-dimensional framework, a decreasing function of the maximum level of damage over the bar was used for the internal length, providing better control of the strains in the localization zone. In fact, the effect of the plastic strain gradient may eventually vanish and the local plasticity and gradient damage model in [Alessi 2013] is recovered, with concentration in the center of the bar and the eventual crack. All of this is obtained with a controllable precursory state.

The results of the viscoplastic regularization are consistent with the results obtained in [Niazi et al. 2013]. In the case of the variational model with nongradient hardening plasticity and gradient damage, the results can be qualitatively compared to [Ambati et al. 2015], where hardening plasticity is also coupled to gradient damage in a different formulation. On the other hand, the effect of the plastic strain gradient shows the same tendency observed in [Dal Corso and Willis 2011]. However, in our model, strains localize and the rest of the bar experiences unloading without introducing perturbations. In addition, the evolution can be prolonged to extreme loading with numerical stability and the narrowing of the localization zone is automatic due to the variable internal length. We think of this behavior as a representation of the necking phenomenon, where the strain localization zone eventually narrows to the fracture point (in our case, the central element of a fine mesh) with a concentration of plastic strains, successfully representing ductile failure.

References

- [Alessi 2013] R. Alessi, *Variational Approach to Fracture Mechanics with Plasticity*, Ph.D. thesis, Université Pierre et Marie Curie-Paris 6, 2013.
- [Alessi et al. 2014] R. Alessi, J.-J. Marigo, and S. Vidoli, “Gradient damage models coupled with plasticity and nucleation of cohesive cracks”, *Arch. Ration. Mech. Anal.* **214**:2 (2014), 575–615.
- [Almansba et al. 2010] M. Almansba, K. Saanouni, and N. E. Hannachi, “Isotropic elastoplasticity fully coupled with non-local damage”, *Engineering* **2**:6 (2010), 420–431.
- [Ambati et al. 2015] M. Ambati, T. Gerasimov, and L. De Lorenzis, “Phase-field modeling of ductile fracture”, *Comput. Mech.* **55**:5 (2015), 1017–1040.
- [Bažant and Jirásek 2002] Z. P. Bažant and M. Jirásek, “Nonlocal integral formulations of plasticity and damage: survey of progress”, *J. Eng. Mech.-ASCE* (2002), 1119–1149.
- [Bigoni 2012] D. Bigoni, *Nonlinear solid mechanics: bifurcation theory and material instability*, Cambridge University Press, 2012.
- [Borja 2013] R. I. Borja, *Plasticity*, Springer, Heidelberg, Germany, 2013.
- [Borst et al. 1993] R. D. Borst, L. Sluys, H. Muhlhaus, and J. Pamin, “Fundamental issues in finite element analyses of localization of deformation”, *Eng. Computation* **10**:2 (1993), 99–121.

- [Bourdin et al. 2008] B. Bourdin, G. A. Francfort, and J.-J. Marigo, “The variational approach to fracture”, *J. Elasticity* **91**:1-3 (2008), 5–148.
- [Chen et al. 2011] Q. Chen, J. E. Andrade, and E. Samaniego, “AES for multiscale localization modeling in granular media”, *Comput. Methods Appl. Mech. Eng.* **200**:33-36 (2011), 2473–2482.
- [Dal Corso and Willis 2011] F. Dal Corso and J. R. Willis, “Stability of strain-gradient plastic materials”, *J. Mech. Phys. Solids* **59**:6 (2011), 1251–1267.
- [De Borst and Mühlhaus 1992] R. De Borst and H.-B. Mühlhaus, “Gradient-dependent plasticity: Formulation and algorithmic aspects”, *Int. J. Numer. Methods Eng.* **35**:3 (1992), 521–539.
- [de Borst et al. 1999] R. de Borst, J. Pamin, and M. G. Geers, “On coupled gradient-dependent plasticity and damage theories with a view to localization analysis”, *Eur. J. Mech., A, Solids* **18**:6 (1999), 939–962.
- [Duda et al. 2015] F. P. Duda, A. Ciarbonetti, P. J. Sánchez, and A. E. Huespe, “A phase-field/gradient damage model for brittle fracture in elastic–plastic solids”, *Int. J. Plasticity* **65** (2015), 269–296.
- [Francfort and Marigo 1998] G. A. Francfort and J.-J. Marigo, “Revisiting brittle fracture as an energy minimization problem”, *J. Mech. Phys. Solids* **46**:8 (1998), 1319–1342.
- [Garikipati and Hughes 1998] K. Garikipati and T. J. R. Hughes, “A study of strain localization in a multiple scale framework—the one-dimensional problem”, *Comput. Methods Appl. Mech. Eng.* **159**:3-4 (1998), 193–222.
- [Jirásek and Rolshoven 2009a] M. Jirásek and S. Rolshoven, “Localization properties of strain-softening gradient plasticity models, I: Strain-gradient theories”, *Int. J. Solids Struct.* **46**:11-12 (2009), 2225–2238.
- [Jirásek and Rolshoven 2009b] M. Jirásek and S. Rolshoven, “Localization properties of strain-softening gradient plasticity models, II: Theories with gradients of internal variables”, *Int. J. Solids Struct.* **46**:11-12 (2009), 2239–2254.
- [Krajcinovic 1989] D. Krajcinovic, “Damage mechanics”, *Mech. Mater.* **8**:2 (1989), 117–197.
- [Lancioni 2015] G. Lancioni, “Modeling the response of tensile steel bars by means of incremental energy minimization”, *J. Elasticity* **121**:1 (2015), 25–54.
- [Lemaitre and Lippmann 1996] J. Lemaitre and H. Lippmann, *A course on damage mechanics*, vol. 2, Springer, Berlin, 1996.
- [Mainik and Mielke 2005] A. Mainik and A. Mielke, “Existence results for energetic models for rate-independent systems”, *Calc. Var. Partial Differential Equations* **22**:1 (2005), 73–99.
- [Maugin 1992] G. A. Maugin, *The thermomechanics of plasticity and fracture*, Cambridge Texts in Applied Mathematics 7, Cambridge University Press, 1992.
- [Maugin and Muschik 1994] G. A. Maugin and W. Muschik, “Thermodynamics with internal variables. II: Applications”, *J. Non-Equilibrium Thermodyn.* **19**:3 (1994), 250–289.
- [Miehe et al. 2010] C. Miehe, F. Welschinger, and M. Hofacker, “Thermodynamically consistent phase-field models of fracture: variational principles and multi-field FE implementations”, *Internat. J. Numer. Methods Eng.* **83**:10 (2010), 1273–1311.
- [Mielke 2006] A. Mielke, “A mathematical framework for generalized standard materials in the rate-independent case”, pp. 399–428 in *Multifield problems in solid and fluid mechanics*, edited by R. Helmig et al., Lect. Notes Appl. Comput. Mech. **28**, Springer, Berlin, 2006.
- [Moës et al. 1999] N. Moës, J. Dolbow, and T. Belytschko, “A finite element method for crack growth without remeshing”, *Int. J. Numer. Methods Eng.* **46**:1 (1999), 131–150.
- [Mumford and Shah 1989] D. Mumford and J. Shah, “Optimal approximations by piecewise smooth functions and associated variational problems”, *Comm. Pure Appl. Math.* **42**:5 (1989), 577–685.
- [Needleman 1988] A. Needleman, “Material rate dependence and mesh-sensitivity in localization problems”, *Comput. Methods Appl. Mech. Eng.* **67**:1 (1988), 69–85.
- [Niazi et al. 2013] M. S. Niazi, H. H. Wisselink, and T. Meinders, “Viscoplastic regularization of local damage models: revisited”, *Comput. Mech.* **51**:2 (2013), 203–216.
- [Oliver et al. 2002] J. Oliver, A. Huespe, M. Pulido, and E. Chaves, “From continuum mechanics to fracture mechanics: the strong discontinuity approach”, *Eng. Fract. Mech.* **69**:2 (2002), 113–136.
- [Oliver et al. 2003] J. Oliver, A. E. Huespe, M. D. G. Pulido, and E. Samaniego, “On the strong discontinuity approach in finite deformation settings”, *Internat. J. Numer. Methods Eng.* **56**:7 (2003), 1051–1082.

- [Oliver et al. 2004] J. Oliver, A. Huespe, E. Samaniego, and E. Chaves, “Continuum approach to the numerical simulation of material failure in concrete”, *Int. J. Numer. Anal. Methods Geomech.* **28**:7-8 (2004), 609–632.
- [Pham and Marigo 2010a] K. Pham and J.-J. Marigo, “Approche variationnelle de l’endommagement. I: Les concepts fondamentaux”, *C. R. Méc. Acad. Sci. Paris* **338**:4 (2010), 191–198.
- [Pham and Marigo 2010b] K. Pham and J.-J. Marigo, “Approche variationnelle de l’endommagement. II: Les modèles à gradient”, *C. R. Méc. Acad. Sci. Paris* **338**:4 (2010), 199–206.
- [Runesson 2006] K. Runesson, “Constitutive modeling of engineering materials, theory and computation”, lecture notes, 2006, [http://www.am.chalmers.se/~ragnar/material_mechanics_home/literature/ThePrimer_\(1\).pdf](http://www.am.chalmers.se/~ragnar/material_mechanics_home/literature/ThePrimer_(1).pdf).
- [Samaniego and Belytschko 2005] E. Samaniego and T. Belytschko, “Continuum-discontinuum modelling of shear bands”, *Internat. J. Numer. Methods Eng.* **62**:13 (2005), 1857–1872.
- [Simo and Hughes 1998] J. Simo and T. Hughes, *Computational inelasticity*, Springer, Berlin, 1998.
- [Triantafyllidis and Aifantis 1986] N. Triantafyllidis and E. C. Aifantis, “A gradient approach to localization of deformation, I: Hyperelastic materials”, *J. Elasticity* **16**:3 (1986), 225–237.
- [Venini and Morana 2001] P. Venini and P. Morana, “An adaptive wavelet-Galerkin method for an elastic-plastic-damage constitutive model: 1D problem”, *Comput. Methods Appl. Mech. Eng.* **190**:42 (2001), 5619–5638.

Received 1 Feb 2016. Revised 4 May 2016. Accepted 19 May 2016.

JACINTO ULLOA: juv1991@gmail.com

Universidad de Cuenca, Av. 12 de Abril s/n, 010203, Cuenca, Ecuador

PATRICIO RODRÍGUEZ: patricio.rodriguez@ucuenca.ec

Universidad de Cuenca, Av. 12 de Abril s/n, 010203, Cuenca, Ecuador

ESTEBAN SAMANIEGO: esteban.samaniego@ucuenca.edu.ec

Facultad de Ingeniería and Departamento de Recursos Hídricos y Ciencias Ambientales, Universidad de Cuenca, Av. 12 de Abril s/n, 010203, Cuenca, Ecuador

JOURNAL OF MECHANICS OF MATERIALS AND STRUCTURES

msp.org/jomms

Founded by Charles R. Steele and Marie-Louise Steele

EDITORIAL BOARD

ADAIR R. AGUIAR	University of São Paulo at São Carlos, Brazil
KATIA BERTOLDI	Harvard University, USA
DAVIDE BIGONI	University of Trento, Italy
YIBIN FU	Keele University, UK
IWONA JASIUK	University of Illinois at Urbana-Champaign, USA
C. W. LIM	City University of Hong Kong
THOMAS J. PENCE	Michigan State University, USA
GIANNI ROYER-CARFAGNI	Università degli studi di Parma, Italy
DAVID STEIGMANN	University of California at Berkeley, USA
PAUL STEINMANN	Friedrich-Alexander-Universität Erlangen-Nürnberg, Germany

ADVISORY BOARD

J. P. CARTER	University of Sydney, Australia
D. H. HODGES	Georgia Institute of Technology, USA
J. HUTCHINSON	Harvard University, USA
D. PAMPLONA	Universidade Católica do Rio de Janeiro, Brazil
M. B. RUBIN	Technion, Haifa, Israel

PRODUCTION production@msp.org

SILVIO LEVY Scientific Editor

Cover photo: Mando Gomez, www.mandolux.com

See msp.org/jomms for submission guidelines.

JoMMS (ISSN 1559-3959) at Mathematical Sciences Publishers, 798 Evans Hall #6840, c/o University of California, Berkeley, CA 94720-3840, is published in 10 issues a year. The subscription price for 2016 is US \$575/year for the electronic version, and \$735/year (+\$60, if shipping outside the US) for print and electronic. Subscriptions, requests for back issues, and changes of address should be sent to MSP.

JoMMS peer-review and production is managed by EditFLOW[®] from Mathematical Sciences Publishers.

PUBLISHED BY

 **mathematical sciences publishers**
nonprofit scientific publishing

<http://msp.org/>

© 2016 Mathematical Sciences Publishers

What discrete model corresponds exactly to a gradient elasticity equation?	VASILY E. TARASOV	329
A refined 1D beam theory built on 3D Saint-Venant's solution to compute homogeneous and composite beams	RACHED EL FATMI	345
A unified theory for constitutive modeling of composites	WENBIN YU	379
Modeling and experimentation of a viscoelastic microvibration damper based on a chain network model	CHAO XU, ZHAO-DONG XU, TENG GE and YA-XIN LIAO	413
An anisotropic piezoelectric half-plane containing an elliptical hole or crack subjected to uniform in-plane electromechanical loading	MING DAI, PETER SCHIAVONE and CUN-FA GAO	433
On the causality of the Rayleigh wave	BARIŞ ERBAŞ and ONUR ŞAHİN	449
On the modeling of dissipative mechanisms in a ductile softening bar	JACINTO ULLOA, PATRICIO RODRÍGUEZ and ESTEBAN SAMANIEGO	463